Composites Science and Technology 57 (1997) 1673–1688

Printed in Northern Ireland
PII: S0266-3538(97)00104-8
0266-3538/98 $19.00

CREEP OF POLYMER COMPOSITES

J. Raghavan[a] & M. Meshii[b]

[a]Department of Mechanical and Industrial Engineering, University of Manitoba, Winnipeg, Manitoba, Canada R3T 5V6
[b]Department of Materials Science and Engineering, Robert R. McCormick School of Engineering, Northwestern University, Evanston, IL 60208, USA

(Received 10 January 1996; revised 4 June 1997; accepted 25 June 1997)

Abstract
A model incorporating a modified thermal activation theory is presented to model and predict creep of polymer composites. Results are presented of the successful application of this model to predict creep of a unidirectional, continuous-carbon-fiber-reinforced polymer composite (AS4/3501-6) and its epoxy matrix, over a wide range of stress (10–80% of ultimate tensile strength) and temperature (295–433 K). From an analysis of model parameters, it is concluded that the reinforcing carbon fibers do not alter the creep mechanism but do alter the creep behavior of the epoxy matrix, resulting in reductions in creep rate and in the magnitude of creep. © *1998 Elsevier Science Ltd. All rights reserved*

Keywords: A. polymer-matrix composites, B. creep, creep rupture, thermal activation theory

1 INTRODUCTION

Two major concerns in using advanced polymer composites in structural applications are their long-term dimensional stability and their long-term strength, as a consequence of the viscoelasticity of the polymer matrix. Information on long-term deformation and strength are normally obtained by extrapolation of short-term test data, obtained under accelerated testing conditions such as higher temperature, stress and humidity, to service conditions by using a prediction model. The accuracy of prediction depends on the accuracy of the model as well as on its validity in the extrapolation range of temperature, stress and time. In an effort to develop an accurate model to predict both creep and creep rupture of polymer composites, the present authors adopted an approach wherein creep rupture was considered to be the termination of creep. Hence, an accurate model to simulate creep and a fracture criterion to predict creep rupture were essential. The former is discussed in this paper while the latter is discussed elsewhere.[1–3]

The creep models that have been used in the past to model the creep of polymers and polymer composites are mechanical analogs, hereditary integrals, Findley's model, Schapery's model, thermal activation theory, the time–temperature–stress superposition principle (TTSSP) and a power law. A review of them is beyond the scope of this paper and can be found in.[1,2,4] These models (except thermal activation theory) were not chosen for this study for one or more of the following reasons: complexity of the model, its unsuitability to non-linear viscoelastic materials or its inability to model the actual time-dependent behavior beyond the experimental time period. Moreover, the TTSSP used in these models (except thermal activation theory), to extrapolate data from one set of conditions to another, assumes that the shape of the compliance versus logarithmic time curve remains the same in the entire range of extrapolation. This may not be valid for many non-linear viscoelastic polymer matrices (as will be seen in this study for the epoxy matrix of the AS4/3501-6 composite) of polymer composites in use today. On the basis of these inferences, thermal activation theory, which has been widely used in the analysis of plastic deformation but has found limited success in the viscoelastic analysis of polymers, was chosen by the present authors to model the creep of the polymer composite. Activation theory is like TTSSP, but it is also applicable to non-linear viscoelastic materials. However, unlike the other models, it is based on a theory that allows correlation of the activation parameters with microscopic phenomena that cause creep and relaxation, thus making this model valuable.

As for a simple activation theory, the macroscopic creep rate will be the product of the number of flow units, the average strain increment per jump over an energy barrier and the probability that each unit would undergo such a jump.[5,6] However, it was successful in the past only in a limited strain-rate/time scale because of the assumption that the number of flow units available for activated transition and the average strain increment per activated transition over the energy barrier remained constant during creep. In reality, the number of flow units available for activated transition and the average strain increment per transition may vary with strain rate. Because of this, previous investi-

gators were unable to use a single activation process to model the entire creep range and they used a spectrum of activation processes to model the creep of the polymer in the entire strain-rate/time range.[7]

In view of the above observation, the present authors adopted an approach wherein the change in the number of flow units available for activated transition and in the strain increment per transition were taken in to account. This approach and its success in modeling and predicting the creep of a unidirectional, continuous-carbon-fiber-reinforced polymer composite (AS4/3501-6) and its epoxy (3501-6) matrix, in a wide range of stress and temperature below the glass-transition temperature, T_g, are presented and discussed in this paper. In addition, the model parameters are analysed to understand the effect of the reinforcing carbon fibers on the creep of the polymer matrix.

2 THEORETICAL MODEL FRAMEWORK

The model framework used, in this study, to model and predict both creep and creep rupture is shown in Fig. 1. When the polymer matrix of a polymer composite is stressed, its free energy is momentarily raised. This is then dissipated gradually when the polymer segments reorient to a lower energy state. This is accomplished by conformational transitions of the molecular bonds and the rate of this process depends on temperature, stress and the cooperative motion among the molecular neighbors.[8] At temperatures far below T_g, the viscous resistance to reorientation of chain segments will be very high so that the polymer matrix behaves like a brittle solid. However, with increase in temperature, the viscous resistance is more frequently overcome and the polymer becomes progressively softer; at temperatures above T_g, it approaches a state where the viscous resistance to reorientation of chain segments is easily overcome. This state of the material is represented by a resistive element with modulus E_R (referred to in this paper as rubbery modulus) in Fig. 1. The viscous resistance to chain segmental reorientation is represented by a resistive element with modulus E_V (referred to here as viscous modulus). The viscous modulus is the magnitude of drop in modulus across the glass transition, i.e. the difference between the instantaneous, E_0, and the rubbery moduli. These moduli were measured by using dynamic mechanical thermal analysis (DMTA).[1] With increase in temperature the viscous resistance in the material is overcome by the conformational transitions, resulting in creep. The modified thermal activation theory used in modeling these thermally activated conformational transitions is represented by a box in Fig. 1.

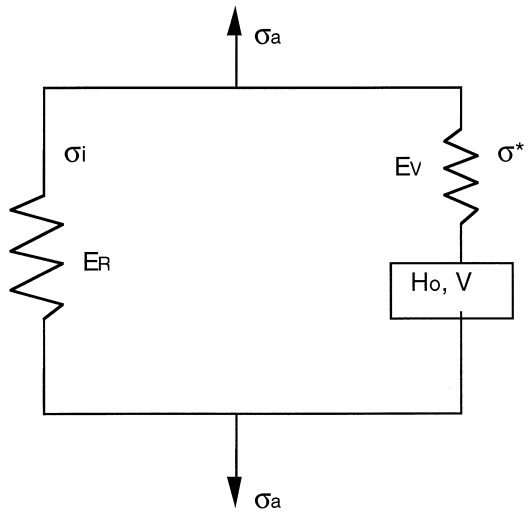

Fig. 1. Schematic of the theoretical model framework.

At a constant temperature, at the instant of application of creep stress, σ_a, to the material, the stresses σ_i and σ^* will be introduced in the resistive elements with modulus E_R and E_V, respectively. σ_i and σ^* are referred in this paper as internal and effective stresses, respectively. The instantaneous creep compliance of the composite is given by the reciprocal of the instantaneous modulus, which is the sum of E_R and E_V. With progress in time, the thermally activated transitions will take place under the action of temperature and σ^*, resulting in an increase in total strain, ε_T, and the creep compliance of the composite will increase as shown in Fig. 2. As creep progresses with time, the internal stress increases and effective stress decreases but maintain the relationship

$$\sigma_a = \sigma_i(t) + \sigma^*(t) \tag{1}$$

The decrease in effective stress, as creep progresses, causes a decrease in creep rate. Finally, provided the material does not fracture, the composite compliance reaches a saturation value as shown in Fig. 2, when the creep rate decreases to zero. This saturation compliance will be the reciprocal of the rubbery modulus.

However, polymers and their composites have been found to fracture before reaching the saturation plateau. The same model framework shown in Fig. 1 was used by the present authors to predict creep rupture by proposing that the composite fractures when the total stored energy in the resistive elements with modulus E_R and E_V reaches a critical value.[2] This critical energy for fracture was measured experimentally by using constant-strain-rate tensile tests at various temperatures. The details of the creep rupture modeling can be found in.[1–3] The details of the creep model based on the model framework shown in Fig. 1 are given in this paper.

Thus a single theoretical model framework as shown in Fig. 1 has been used to model and predict both creep and creep rupture of the polymer composite and its epoxy matrix. A mechanical analog similar to one shown in Fig. 1 was first used by Eyring and Halsey[9] to model the constant-strain-rate behavior of textile fibers. Since then, several combinations of such mechanical

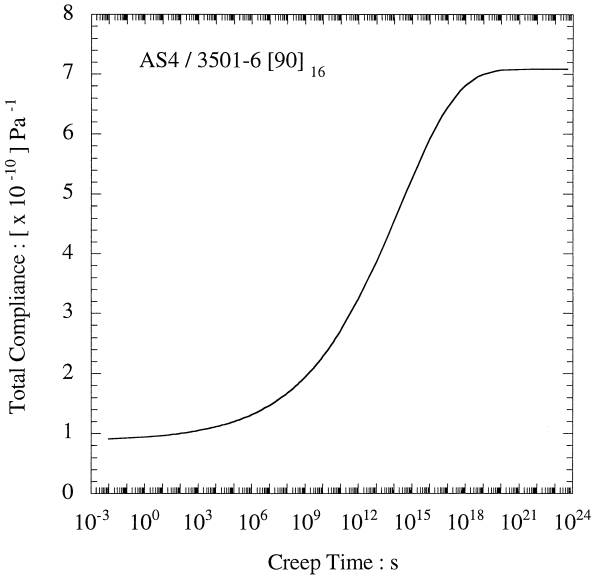

Fig. 2. Simulated compliance curve for composite using the model framework given in Fig. 1. The curve beyond a reasonable time period of 10^9 s is shown to point out that the composite compliance will saturate to a plateau value if fracture does not occur during this time period.

analogs have been used by several investigators to empirically fit the experimental creep data. However, the modified thermal activation theory differentiates the present approach from the earlier ones. In addition, in contrast to earlier approaches, the model parameters in this model were measured by individual experiments.

2.1 Creep

A detailed derivation of the analytical expression for creep by using the modified thermal activation theory can be found in.[1] A brief discussion of this derivation is provided below.

The polymer chain segmental motion that results in macroscopic creep strain is represented by the box in Fig. 1. This is modeled by thermal activation theory to be a rate process of overcoming an energy barrier, as shown in Fig. 3. G_0 is the height of the energy barrier separating the two energy states 1 and 2 and is known as the free energy of activation. In the absence of stress, the available thermal energy, at a temperature T, will cause the polymer segmental units to overcome the energy barrier in both forward and backward directions. When a stress is applied, the work done by it contributes towards surmounting the energy barrier preferentially in one direction. Here it is assumed that stress aids in the transition from state 1 to state 2. Considering the transition in both the forward and backward directions, the net strain rate is given[5,6] by

$$\dot{\epsilon}_V = \dot{\epsilon}_0 \exp\left(-\frac{H_0}{kT}\right) \sinh\left(\frac{v\sigma^*}{kT}\right) \tag{2a}$$

where ϵ_0 is the pre-exponential factor given by

$$\epsilon_0 = 2N_1 \Delta\epsilon \frac{kT}{h} \exp\left(\frac{S_0}{k}\right) \tag{2b}$$

T is the test temperature, k is Boltzmann's constant, h is Planck's constant, N_1 is the number of chain segmental units (referred to in this paper as flow units) in state 1 and $\Delta\epsilon$ is the macroscopic strain increment per transition from state 1 to state 2. The transmission coefficient is taken to be unity. Here G_0 is written in terms of H_0, the enthalpy of activation, which is also referred to as the activation energy at zero effective stress for the transition process, and S_0, the entropy of activation which is assumed to be constant in the entire temperature range of investigation. v is the stress coefficient and is referred to as activation volume since its units are same as that of volume. This was measured experimentally by means of tensile tests at both differential and constant strain rates. In metals, this volume has been shown to be equal to the product of the area swept by a dislocation while overcoming an energy barrier and the Burger's vector of the dislocation. However, no such clear definition exists for polymers. Basinski[10] and Conrad and Widersich[11] proposed that only a part of the applied stress assisted the dislocation in overcoming the energy barrier. This part of applied stress, referred to as the effective stress, σ^*, is derived by subtracting the internal stress from the applied stress as per eqn (1). Previous investigators had deduced this effective stress in polymers by measuring the internal stress in stress-dip tests[12] and stress-relaxation tests.[13] However, such testing in polymer composites is scarce with the exception of work by Pink and Campbell.[14,15] Raghavan and Meshii[7] measured this internal stress by step-unloading tests and by stress-relaxation tests. However, the measured internal stress values were considered to be

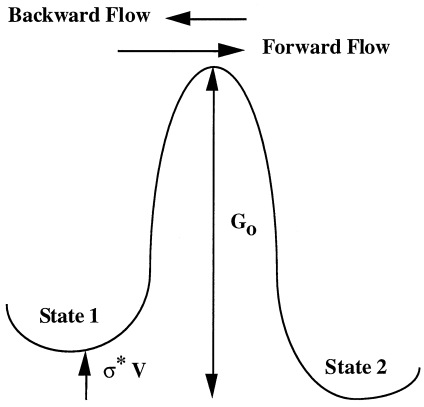

Fig. 3. Schematic of an energy barrier separating two energy states, 1 and 2, in the polymer-matrix composite. $\sigma^* V$ is the work done by the effective stress in overcoming the energy barrier in the forward direction.

apparent values owing to the influence of transient effects and errors involved in the extrapolation method.[1] Hence, in this approach, the difficulty associated with direct determination of internal stress was avoided by defining the internal stress at any macroscopic strain by E_R, which was measured by means of DMTA.

By using this simple activation theory within the model framework given in Fig. 1, previous investigators could successfully model the creep of polymers only in a limited strain rate range owing to the assumption that N_1 and $\Delta\epsilon$ remained constant during the entire strain-rate/creep-time range. Earlier attempts,[4,16] including a change in N_1 with creep rate, assuming a constant $\Delta\epsilon$, were not successful in modeling the actual creep/relaxation behavior of polymers. The approach used in this paper, allowing both N_1 and $\Delta\epsilon$ change with strain rate, is described below.

Referring to Fig. 3, the total number of flow units, N, available in both state 1 and state 2, is given by

$$N = N_1 + N_2 \tag{3}$$

N remains constant since the total population of flow units cannot change. The number of flow units N_1 is written as

$$N_1 = N_1^0 - X \tag{4}$$

where N_1^0 is the magnitude of N_1 at the instant of application of creep stress σ_a. X is the total change in N_1 from the start of creep until a certain strain (creep) rate. Corresponding to this change, there would be an increase in macroscopic strain and a decrease in effective stress, $\Delta\sigma^*$. Since X cannot be directly measured, it has to be derived indirectly through their relationship with the decrease in effective stress or effective stress, σ^*, remaining in the material at a strain rate.

In polymers, the conformational transition of a flow unit from state 1 to state 2 is dependent on the cooperative mobility of the neighboring flow units since all of them are part of a long chain (in contrast, in metals the dislocation mobility is independent of the adjacent dislocations although there can be interactions among them). Since there is no known mathematical form or theory describing the cooperative mobility and thus the number of flow units, ΔX, going over the energy barrier from state 1 to state 2 at a strain rate and ΔX as a function of strain rate (creep time) to yield the distribution in X in the entire strain rate (creep time) range, the functional form for the relationship between X and $\Delta\sigma^*$ or σ^* in the entire strain rate (creep time) range has to be derived phenomenologically from creep/relaxation experiments. Since the cooperative mobility and thus ΔX cannot be described in deterministic terms, the distribution in X can be given only in probabilistic terms.

On the basis of experimental creep and relaxation data for various polymers and composites and the success of the well-known Kohlrausch–Williams–Watts (KWW) equation in modeling the stage 1 relaxation in polymers,[8] the present authors decided that a Weibull distribution in X would be most appropriate to generate a creep curve that would closely resemble the experimental creep curve. Moreover, the mathematical form of the KWW equation resembles that of the Weibull distribution, which has been successful in modeling the time-dependent failure in materials.[17] Hence, a Weibull distribution in X is assumed. Let $P(X)$ be the probability that the total change in N_1, from the start of creep until a certain creep rate, is equal to X. It is given by

$$P(X) = 1 - \exp\left\{-\left[\left(\frac{X}{X_0}\right)^{\beta}\right]\right\} \tag{5a}$$

The decrease in effective stress is given by

$$\Delta\sigma^* = P(X)\sigma_0^* \tag{5b}$$

where σ_0^* is the effective stress in the material at the instant of application of the load and

$$\Delta\sigma^* = \sigma_0^* - \sigma^* \tag{5c}$$

By using eqns (5a–c), the effective stress remaining in the material, after a change in N_1 by X, can be written as

$$\frac{\sigma^*}{\sigma_0^*} = \exp\left\{-\left[\left(\frac{X}{X_0}\right)^{\beta}\right]\right\} \tag{5d}$$

X_0 represents the total change in N_1 when the effective stress in the material has reduced to σ_0^*/e. β is the Weibull shape factor. With progress in creep, X increases and N_1 decreases. Hence, the effective stress in the material decreases according to eqn (5), causing a decrease in creep rate.

From eqn (5d)

$$\frac{d\sigma^*}{dX} = -\beta\frac{\sigma^*}{X_0}\left[-\ln\left(\frac{\sigma^*}{\sigma_0^*}\right)\right]^{1-\frac{1}{\beta}} \tag{6}$$

By using eqn (4), $\Delta\epsilon$ in eqn (2b) can be written as

$$\Delta\epsilon = \frac{d\epsilon}{dN_1} = -\frac{d\epsilon}{dX} = -A'\frac{d\sigma^*}{dX} \tag{7}$$

where A' is a constant. Substituting eqn (6) in eqn (7) gives

$$\frac{d\epsilon}{dN_1} = A'\beta\frac{\sigma^*}{X_0}\left[-\ln\left(\frac{\sigma^*}{\sigma_0^*}\right)\right]^{1-\frac{1}{\beta}} \tag{8}$$

From Fig. 1, it can be shown that

$$A' = \frac{E_R + E_V}{E_V E_R} \tag{9}$$

The initial population of units in state 1 and state 2, i.e. N_1^0 and N_2^0 respectively at the instant of application of stress, will change due to creep and reach a final population of N_1^∞ and N_2^∞ in states 1 and 2 respectively when the material reaches the rubbery state and the material's compliance reaches a plateau value. Obviously, only a certain number of flow units in state 1 will be participating in the conformational transition from state 1 to state 2. Hence, it is assumed that only a certain number of flow units, ΔN_1, would be available out of N_1, at a strain rate, with the same conformational transitional probability. Owing to the dependence on cooperative mobility of neighboring flow units, ΔX units out of ΔN_1 may actually undergo transition from state 1 to state 2 at a given strain rate (creep time). Since it is likely that $\Delta X \ll \Delta N_1$ (and $\Delta N_1 > X^\infty$, which is the total change in N_1 by the end of creep), it is assumed that the value of ΔN_1 remains constant in the entire strain-rate range. Substituting for ΔN_1, eqn (8) and (9) in eqn (2), the following relationship is obtained for creep rate:

$$\dot{\epsilon}_V = \dot{\epsilon}_0' \sigma^* \left[-\ln\left(\frac{\sigma^*}{\sigma_0^*}\right) \right]^{1-\frac{1}{\beta}} \exp\left(-\frac{H_0}{kT}\right) \sinh\left(\frac{v\sigma^*}{kT}\right) \tag{10a}$$

where

$$\dot{\epsilon}_0' = 2\frac{E_R + E_V}{E_R E_V} \frac{\Delta N_1}{X_0} \beta \frac{kT}{h} \exp\left(\frac{S_0}{k}\right) \tag{10b}$$

It can be inferred from Fig. 1 that during creep, in addition to viscous strain rate, there will also be an elastic strain rate due to the time-dependent change in elastic strain in element E_V. Hence, the total creep rate measured during a constant-stress creep experiment is written as

$$\dot{\epsilon}_T = \dot{\epsilon}_e + \dot{\epsilon}_V \tag{11}$$

where

$$\dot{\epsilon}_T = \left(\frac{1}{E_R}\right)\frac{d\sigma_i}{dt} \quad \text{and} \quad \dot{\epsilon}_e = \left(\frac{1}{E_V}\right)\frac{d\sigma^*}{dt} \tag{12}$$

With these definitions and eqn (1), since $d\sigma_a/dt = 0$, eqn (10a) can be written as

$$\dot{\epsilon}_T = B\sigma^* \left[-\ln\left(\frac{\sigma^*}{\sigma_0^*}\right) \right]^{1-\frac{1}{\beta}} \exp\left(-\frac{H_0}{kT}\right) \sinh\left(\frac{v\sigma^*}{kT}\right) \tag{13a}$$

where

$$B = 2\left(\frac{1}{E_R}\right)\frac{\Delta N_1}{X_0}\beta\frac{kT}{h}\exp\left(\frac{S_0}{k}\right) \tag{13b}$$

In this paper, eqn (13) is called the creep prediction equation and was used to model and predict the creep of polymer composites and its epoxy matrix. The method of experimental verification of this model is explained in the next section.

2.2 Details on creep modeling and prediction

In this study, all model parameters except the pre-exponential factor, B, and the Weibull shape factor, β, are either directly measurable by experiments or can be indirectly derived from experimental results. Hence, the values of the pre-exponential factor and Weibull shape factor were obtained by numerical fitting of the experimental creep curves using the creep prediction equation according to the following procedure.

The total experimental strain measured as a function of time, at an applied stress of σ_a, was used to calculate the creep rate. The effective stress was calculated as follows. At a macroscopic strain, the internal stress was calculated by the product of strain and the rubbery modulus, E_R. Subtracting this internal stress from the applied stress, the effective stress corresponding to the macroscopic strain and strain rate was obtained. This resulted in experimental creep rate versus effective stress results. From the product of instantaneous strain and rubbery modulus, the internal stress at the instant of application of load was obtained. Then, σ_0^* was calculated by subtracting this internal stress from the applied stress. The activation volume v was derived from tests conducted at differential and constant strain rates and was found to be modeled by the following analytical form

$$\frac{v}{T} = C(\sigma^*)^{-D} \tag{14}$$

where T is the temperature, C and D are constants. Activation energy was derived from DMTA test results. By using eqns (13) and (14), activation energy and instantaneous effective stress, the experimental creep rate results were numerically fitted to obtain the model parameters B and β. The above procedure was repeated for creep results obtained at different stress levels and temperatures to obtain the values of B and β at different creep stress levels and temperatures.

With these model parameters, the creep compliance curve, at a given temperature and applied stress, was calculated numerically[1] to obtain total strain values as function of time. The total time-dependent creep compliance was calculated with the following relationship:

$$S(t) = \frac{\epsilon_T(t)}{\sigma_a} \tag{15}$$

The calculated compliances were compared with the experimental creep compliances at different stress levels and temperatures to verify the modeling capability of

the creep model and the accuracy of numerical fitting used to obtain B and β. The experimental creep results measured on specimens with fibers oriented at 0°, 90° and 10° to the loading axis were modeled with the creep model to obtain the analytical form of the creep compliances in the compliance matrix given below:

$$\begin{bmatrix} S_{11}(t) & S_{12}(t) & 0 \\ S_{12}(t) & S_{22}(t) & 0 \\ 0 & 0 & S_{66}(t) \end{bmatrix} \tag{16}$$

Finally, to verify the predictive capability of the creep model, the creep compliance for the unidirectional composite specimen with fibers oriented at an arbitrary angle, θ, to the loading axis was predicted by using the above compliance matrix and the following equation:[18]

$$S_\theta = S_{11}(\cos\theta)^4 + [S_{66} - (2\nu_{12}S_{11})](\cos\theta)^2(\sin\theta)^2 + S_{22}(\sin\theta)^4 \tag{17}$$

where ν_{12} is the Poisson's ratio. The results predicted for off-axis specimens by means of this equation were compared with the experimental results for composites with fibers oriented at 30° and 60° to the loading axis.

3 EXPERIMENTAL DETAILS

3.1 Material

Continuous-carbon-fiber-reinforced polymer composite (AS4/3501-6) and its epoxy (3501-6) matrix were used to verify the ability of the creep model to simulate creep. AS4/3501-6 prepregs were supplied by Hercules Corporation, Magna, Utah. Laminates were made in-house in an autoclave.[1] Eight plies were used for [0], [10], [30] and [60] laminates, while 16 plies were used for [90] laminates. The fiber volume fraction after curing was 0·62. The $[0]_8$, $[10]_8$ and $[90]_{16}$ laminates were used to measure longitudinal, shear and transverse properties, respectively. The $[30]_8$ and $[60]_8$ laminates were used to verify the predictions of the creep model.

Tensile test coupons of size 165 mm in length and 12·7 mm in width were cut from the laminate plates with a diamond saw, wet ground with SiC papers, polished with 1 mm diamond paste, rinsed in water and dried. Low-carbon steel tabs 38·1 mm in length and 12·7 mm in width were bonded to the test coupons with AF-191 structural adhesive, supplied by 3M Company. The adhesive was cured at 450 K in a hot press. Resistance strain gages of types EA and WK, supplied by Micro Measurements Inc., North Carolina, were used to measure the strain at room temperature and high temperatures respectively. The EA-type strain gage was bonded with M-bond 200 and cured at room temperature. The WK-type gage was bonded with M-bond 610, which cured at 433 K for 1 h under the pressure of a spring clamp. All the specimens were post-cured at 450 K for 1 h and then cooled slowly to room temperature. The specimens were then stored at laboratory conditions (23°C and an average relative humidity of 50%) for 1 day before testing. This ensured that all the test coupons were in the same physically aged condition before testing. It is believed that any residual stress induced during the curing stages would have been minimized by the annealing step during post-cure operation. The test coupons for 3501-6 epoxy, milled out of the cured plate, were of size recommended by ASTM D638. Resistance strain gages were used to measure the strain. The data were logged during the tests by using a data-acquisition system built into a 386 SX computer.

3.2 DMTA tests

This test was performed on the 3501-6 resin and its composites with different fiber orientations, to measure the glass-transition temperature (T_g), the activation energy (H_0), the instantaneous modulus (E_0), its temperature dependence and the rubbery modulus (E_R). Testing was performed with a Seiko 983 Dynamic Mechanical Analyzer. The epoxy and composite specimens used were approximately 20 mm in length, 1·5 mm in width and 0·5 mm in thickness. The tests were performed in the frequency range of 0·1 Hz to 50 Hz and in the temperature range from 173 K to 573 K. The rate of heating was 1 K min^{-1} and the strain amplitude was 5×10^{-5}. The temperature at which the $\tan\delta$ reached a peak at a frequency of 1 Hz was defined to be the T_g. Assuming that the frequency and the temperature corresponding to the peak in the $\tan\delta$ curve are related by an Arrhenius relationship, the activation energy was calculated from the slope of the frequency versus inverse temperature plot.[1,4] At a temperature of 40 K above T_g, the $\tan\delta$ value approached zero and the modulus value reached a plateau; this plateau value was taken to be the rubbery modulus. The instantaneous modulus was defined to be the storage modulus measured at or above a frequency of 10 Hz at temperatures below 433 K, and its temperature dependence was measured. Since rubbery modulus is proportional to temperature, its value at a temperature was calculated from the product of modulus at T_g+40 and the ratio of that temperature to T_g+40. By subtracting the rubbery modulus from the instantaneous modulus, the viscous modulus was derived. With these modulus values, the effective stress was calculated as explained in the previous section on modeling.

3.3 Constant-strain-rate tests

The tests were performed in Sintec 20/G screw-driven machine at strain rates in the range from 10^{-2} to 10^{-4} s^{-1} at temperatures in the range from 295 K to 463 K. At any given strain, the difference in applied

stress at the two strain rates used in tensile testing was determined from the experimental stress/strain results obtained by tensile testing. Then, the activation volume was determined from the relationship:[5]

$$v = \left(\frac{\mathrm{d}H}{\mathrm{d}\sigma^*}\right)_{T,\text{Structure}} = kT\left(\frac{\partial \ln \dot{\epsilon}}{\partial \sigma_a}\right)_{T,\text{Structure}} \quad (18)$$

where $\dot{\epsilon}$ is the strain rate and σ_a is the applied stress. In deriving eqn (18) using eqn (2), the pre-exponential factor was assumed to be a constant. The implications of this assumption are discussed in.[1] To avoid the influence of variation in modulus from specimen to specimen, a single specimen was used to obtain stress/strain curves at the two strain rates. Two specimens were used at each temperature to obtain the activation volume.

3.4 Creep tests

These tests were performed by using a 2320 lever-arm tester of Applied Test System Inc. All the test coupons were loaded to the desired creep stress at an apparent strain rate of $10^{-4}\,s^{-1}$ after they had equilibrated at the respective test temperatures, i.e. 295 K, 373 K, 403 K and 433 K. The creep stresses chosen for the tests were in the range of 10 to 80% of the ultimate tensile strengths at the respective temperatures. The maximum time of creep at all temperatures was 24 h. At a single temperature, one test coupon was used. Initially, repeated creep tests were performed on a single test coupon to ensure that the creep strains were reproducible.[1] The macroscopic creep strains were recoverable.

4 RESULTS

In this section, experimental, derived and predicted results are presented.

4.1 DMTA test results

4.1.1 Activation energy and glass-transition temperature
The activation energy, H_0, and glass-transition temperatures, T_gs, for the composite with different fiber orientations are given in Table 1 along with the values for the pure 3501-6 epoxy for comparison. The T_g of the composite is higher than that of the pure epoxy (512 K) by 5 to 11 K depending on the orientation of the fiber. The activation energies for both the pure resin as well as the $[0]_8$ and $[90]_{16}$ composites, wherein only tensile strains are introduced by the applied stress, are the same. However, the activation energies of the $[10]_8$ and $[45]_8$ composites, wherein both tensile and shear strains are introduced by the applied stress, are 10 to 14% higher. Activation energies of $495\,kJ\,mol^{-1}$ and $543\,kJ\,mol^{-1}$ were used to simulate the transverse and shear creep curves, respectively.

4.1.2 Instantaneous, viscous and rubbery moduli
The ratio of the instantaneous modulus, E_0, to rubbery modulus, E_R, as measured by DMTA is tabulated in Table 1 for the composites and unreinforced epoxy. The instantaneous (storage) modulus at 295 K and rubbery (storage) modulus at $T_g + 40$ K are considered to be equal to the complex moduli (E) at the respective temperatures of measurement, since the loss moduli at these temperatures are negligible.[1] Hence, in theory, the magnitude of the two moduli measured in DMTA tests on thin specimens should be equal to the magnitude of the moduli of bulk specimens measured in constant-strain tensile tests provided the testing rate and temperature are chosen such that no energy is dissipated during tensile testing, i.e. all the work is stored in the material. In this study, a constant strain rate of $10^{-2}\,s^{-1}$ or higher was chosen to be the testing condition that yielded negligible energy dissipation during testing, i.e. the work done by the applied stress was completely stored. A frequency of 10 Hz, which resulted in a negligible energy loss at extreme temperatures in DMTA testing, translates into a strain rate of $10^{-3}\,s^{-1}$. In DMTA tests a strain amplitude of 5×10^{-5} was used. The above strain rate was calculated by using this strain amplitude. Since the strain amplitudes used in tensile tests were much larger than this, a strain rate higher than this strain rate used in the DMTA test was chosen to yield a condition of zero energy loss while testing. The highest magnitude of $10^{-2}\,s^{-1}$ was chosen owing to the limitations in the testing machine.

However, the magnitude of E_0 measured by tensile tests on bulk test coupons at this strain rate of $10^{-2}\,s^{-1}$ was higher than the E_0 value measured by DMTA in both epoxy and composites by a factor in the range of 1·33 to 1·51, depending on the material. Possible reasons for this difference are as follows:

Table 1. DMTA test results for primary α transition in the 3501-6 epoxy and unidirectional composite with different fiber orientations

Material	Glass-transition temperature, T_g (K)	Tan δ_{max} at a frequency of 1 Hz	Experimental activation energy ($kJ\,mol^{-1}$)	$\frac{E_0}{E_R}$
3501-6 epoxy	512	0·627	493	103·2
AS4/3501-6 $[90]_{16}$	518	0·208	495	7·7
AS4/3501-6 $[0]_8$	517	0·221	504	9·1
AS4/3501-6 $[10]_8$	523	0·131	543	8·3
AS4/3501-6 $[45]_8$	518	0·242	562	16·7

1. The strain range over which the modulus of the bulk specimens was measured was 1×10^{-3}, and this is higher than the strain amplitude used in DMTA tests. This may be the reason for the difference in the measured modulus values at the two strain rates, i.e. 10^{-2} and $10^{-3}\,s^{-1}$. Any dynamic effect of higher strain rate on measured modulus is neglected here.
2. Since the DMTA test coupons are very thin (2 mm in width and 0·5 mm in thickness), a possible variation of both thickness and width along the length of the test coupons could lead to such a difference in moduli. A corollary of this is that a small error in measurement of test coupon dimensions could also lead to this difference.
3. In the case of composites, the resin-to-fiber volume ratio in the DMTA test coupon may be different from that in the bulk test coupon. This may arise as a consequence of the preparation process of the test coupons as well as because of a heterogeneous distribution of fibers in the composite.

To avoid the third reason the DMTA test coupons were cut from the center of the cured laminates, away from the edges. Moreover, the test coupon preparation process was kept uniform for both tensile and DMTA test coupons. Since the magnitude of difference was observed in the epoxy also, where a change in resin-to-fiber volume ratio is not a concern, the authors are inclined to think that the variation could not be due to reason (3).

However, the magnitude of modulus drop owing to the glass-to-rubber transition, i.e. the ratio of instantaneous to rubbery modulus, should not change from thin to bulk samples, since this drop is due to an intrinsic transition process in the epoxy matrix and any geometrical effects that influence the magnitude of both moduli would cancel out in the ratio. Hence, the ratio tabulated in Table 1 was used along with the instantaneous modulus measured during tensile tests at $10^{-2}\,s^{-1}$ to derive the rubbery and viscous moduli of the bulk specimens. The moduli for epoxy and the $[0]_8$, $[10]_8$ and $[90]_{16}$ composites are tabulated in Tables 2–5, respectively. The moduli values for the composite under in-plane shear loading were determined from eqn (17), Tables 3–5 and the experimentally measured Poisson's ratio of 0·31 in the temperature range 295–433 K.[1] These shear moduli values are tabulated in Table 6. Values in Tables 2,3,5 and 6 were used in the modeling and prediction of creep.

4.2 Constant-strain-rate tensile test results

4.2.1 Instantaneous modulus

The instantaneous modulus of bulk specimens, measured at a strain rate of $10^{-2}\,s^{-1}$, was used along with the DMTA test results to calculate the viscous and rubbery moduli of bulk specimens as per the procedure discussed in Section 4.1.2.

4.2.2 Activation volume

Since eqn (18) contains a temperature term, the experimental activation volume was normalized with temperature to delineate the effect of temperature. The activation volume varied inversely with effective stress at a temperature. Although the activation volume versus effective stress plots at all temperatures exhibited nearly the same slope, they did not exhibit a regular trend to delineate the effect of temperature on activation volume. Hence, the activation volume values at temperatures in the range from 295 K to 463 K were con-

Table 2. Instantaneous, rubbery and viscous modulus for 3501-6 epoxy

Specimen	T (K)	Instantaneous modulus, E_0 (GPa)	Rubbery modulus, E_R (GPa)	Viscous modulus, E_V (GPa)
3501-6 resin	295	6·50	0·034	6·47
	373	5·38	0·043	5·33
	403	4·93	0·046	4·88
	433	4·48	0·049	4·43
	463	4·03	0·053	3·98
	552		0·063	

Table 3. Instantaneous, rubbery and viscous modulus for AS4/3501-6 $[0]_8$ composite

Specimen	T (K)	Instantaneous modulus, E_0 (GPa)	Rubbery modulus, E_R (GPa)	Viscous modulus, E_V (GPa)
AS4/3501-6 $[0]_8$ composite	295	200·0	12·7	187·3
	373	196·0	16·1	179·9
	403	195·6	17·4	178·2
	433	193·1	18·7	174·4
	463	191·6	19·9	174·4
	563		24	

Table 4. Instantaneous, rubbery and viscous modulus for AS4/3501-6 $[10]_8$ composite

Specimen	T (K)	Instantaneous modulus, E_0 (GPa)	Rubbery modulus, E_R (GPa)	Viscous modulus, E_V (GPa)
AS4/3501-6 $[10]_8$ composite	295	146·44	8·44	138·00
	373	133·26	10·67	122·59
	403	129·18	11·53	117·65
	433	124·80	12·39	112·42
	463	120·44	13·25	107·20
	563		16·11	

Table 5. Instantaneous, rubbery and viscous modulus for AS4/3501-6 $[90]_{16}$ composite

Specimen	T (K)	Instantaneous modulus, E_0 (GPa)	Rubbery modulus, E_R (GPa)	Viscous modulus, E_V (GPa)
AS4/3501-6 $[90]_{16}$ composite	295	14·00	0·97	13·04
	373	13·20	1·22	11·98
	403	12·92	1·32	11·60
	433	12·62	1·41	11·21
	463	9·52	1·51	8·01
	558		1·82	

Table 6. Instantaneous, rubbery and viscous shear modulus for AS4/3501-6 composite

Specimen	T (K)	Instantaneous shear modulus, E_0 (GPa)	Rubbery shear modulus, E_R (GPa)	Viscous shear modulus, E_V (GPa)
AS4/3501-6 composite	295	14·73	0·72	14·02
	373	13·57	0·90	12·66
	403	12·99	0·98	12·02
	433	12·55	1·05	11·51
	463	12·12	1·12	10·99
	563		1·36	

sidered to be the same, subject to a scatter band as shown in Figs 4–6 for the epoxy, $[90]_{16}$ and $[10]_8$ composites, respectively. The actual experimental data can be found in.[1,19] The upper and lower limits, shown as solid lines in these figures, correspond to highest and lowest activation volume values. At a given effective stress, these limits were separated by a factor of 2·8 for the epoxy and $[90]_{16}$ composite and by a factor of 10 for the $[10]_8$ composite. The power-law constants, obtained by fitting these upper and lower limits using eqn (14), are tabulated in Table 7. The same values for the constants indicate that the activation volume is the same for 3501-6 epoxy and for the $[90_{16}$ composite, whose properties are matrix-dominated. During modeling, the activation volume was allowed to vary between these limits.

4.3 Creep test results

The tensile creep compliance of the epoxy, at creep stresses of 5 and 15 MPa in the temperature range from 295 to 433 K, are given in Figs 7 and 8. The transverse creep compliance, S_{22}, and shear creep compliance, S_{66}, of the AS4/3501-6 composite obtained at various creep stresses are given in Fig. 9–12. The creep of the composite and its epoxy matrix increases with increase in stress, temperature and time. At a given temperature and creep time, it can be observed that the compliance values at two stresses are not the same, i.e. the composite is non-linear in behavior, and that this non-linearity increases with increase in temperature. Moreover, the slope of the compliance curves changes with stress and temperature, indicating that the non-linearity may increase with time. These results verify that the composite is a non-linear material, i.e. it is thermo-rheologically complex in behavior. Comparing Figs 8 and 9, it can be inferred that the magnitude of strain as well as the extent of creep acceleration by stress and temperature in the epoxy is reduced by the reinforcing fibers. Moreover, a comparison of tensile and shear creep compliances reveals that the creep of the composite

Table 7. Power-law constants obtained by fitting the experimental activation volume values using eqn (14)

Material	Power-law constant C		Power-law constant D
	upper limit	lower limit	
3501-6 epoxy	$7{\cdot}2\times10^{-22}$	$2{\cdot}6\times10^{-22}$	1·057
AS4/3501-6 $[90]_{16}$	$7{\cdot}2\times10^{-22}$	$2{\cdot}6\times10^{-22}$	1·061
AS4/3501-6 $[10]_8$	$3{\cdot}5\times10^{-21}$	$3{\cdot}6\times10^{-22}$	1·061

under in-plane shear loading is higher than that under tensile loading. In Figs 7 and 8, the slope of the experimental compliance data at temperatures of 403 K and 433 K appears to decrease at creep times beyond 10 000 s as compared with the slope at creep times less than 10 000 s. The reason for this is not known at this time. However, it is believed that this would have not affected the model parameters, obtained by modeling, owing to relatively few data points beyond 10 000 s.

The creep compliances of the off-axis $[30]_8$ and $[60]_8$ composites, measured at a creep stress of 29·7 MPa, are given in Figs 13 and 14. The resolved in-plane shear stress being the same (12·9 MPa), the higher resolved transverse stress in the $[60]_8$ composite (22·3 MPa) as compared with the $[30]_8$ composite (7·4 MPa) resulted in a higher magnitude of creep in the former than in the latter. In Fig. 14, the total compliance at 433 K is smaller than at 403 K below 800 s. This is believed to result from an anomaly in the experimentally measured instantaneous strains. A single specimen was used at all the three temperatures of testing. The creep test was performed at 295 K in the beginning, followed by testing at 403 K and finally at 433 K. If some sort of progressive damage had occurred during this testing, then the compliance measured at 433 K would be expected to be higher but not lower than the value at 403 K. Hence, this anomaly is not due to the material but is thought to arise from variation in the loading condition while loading to the creep stress of 29·7 MPa. Nevertheless, this anomaly does not influence the time-dependent compliance results.

4.4 Creep modeling results

4.4.1 Pre-exponential factor and Weibull shape factor

A representative experimental creep rate versus effective stress curve is shown in Fig. 15. This curve is

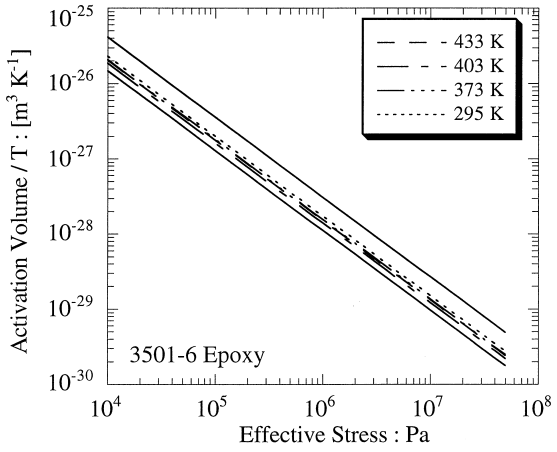

Fig. 4. Activation volume values (broken lines) used in the numerical fitting of experimental creep curves for the epoxy. The solid lines denote the upper and lower bounds.

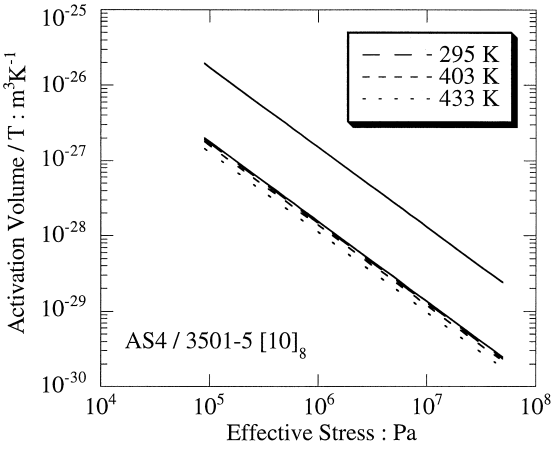

Fig. 6. Activation volume values (broken lines) used in the numerical fitting of experimental shear creep curves for the composite. The solid lines denote the upper and lower bounds.

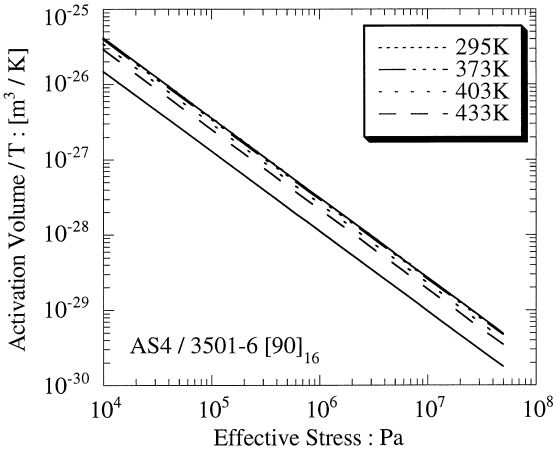

Fig. 5. Activation volume values (broken lines) used in the numerical fitting of experimental transverse creep curves for the composite. The solid lines denote the upper and lower bounds.

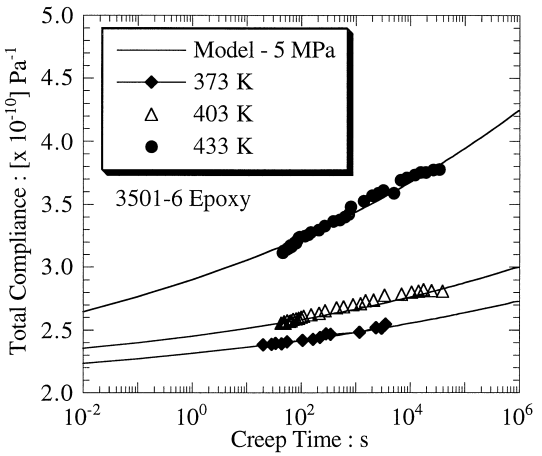

Fig. 7. Comparison of experimental and model fit compliance of the epoxy at a creep stress of 5 MPa.

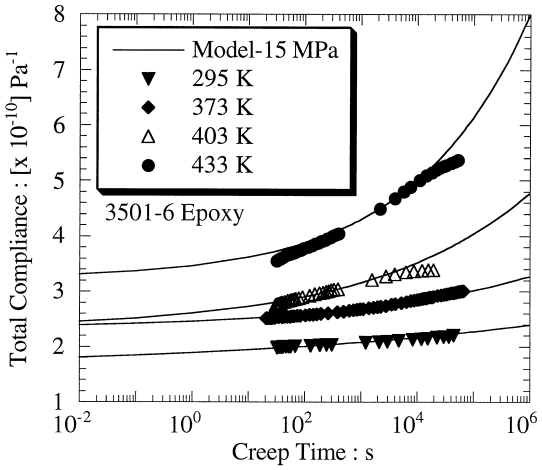

Fig. 8. Comparison of experimental and model fit compliance of the epoxy at a creep stress of 15 MPa.

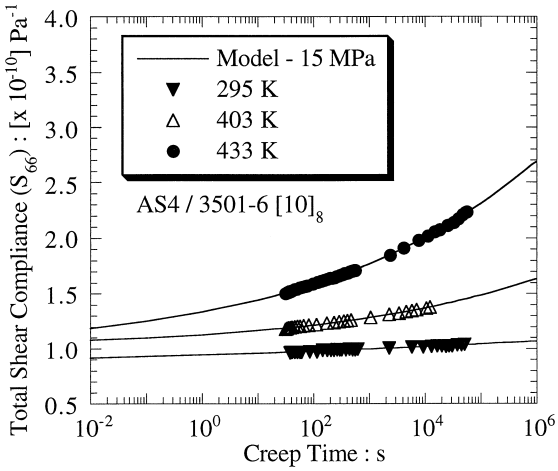

Fig. 11. Comparison of experimental and model fit shear compliance of the composite at a creep stress of 15 MPa.

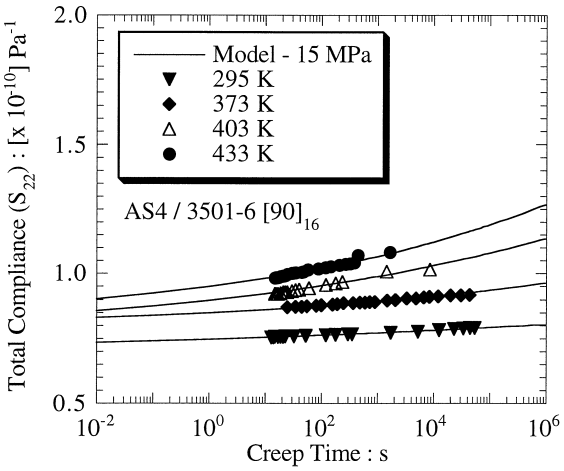

Fig. 9. Comparison of experimental and model fit transverse compliance of the composite at a creep stress of 15 MPa.

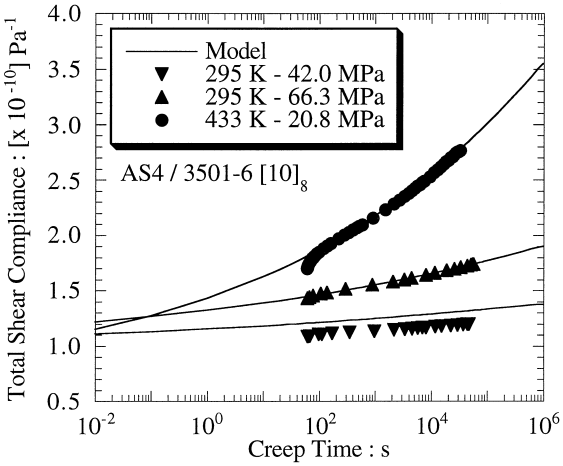

Fig. 12. Comparison of experimental and model fit shear compliance of the composite at a different creep stresses and temperature.

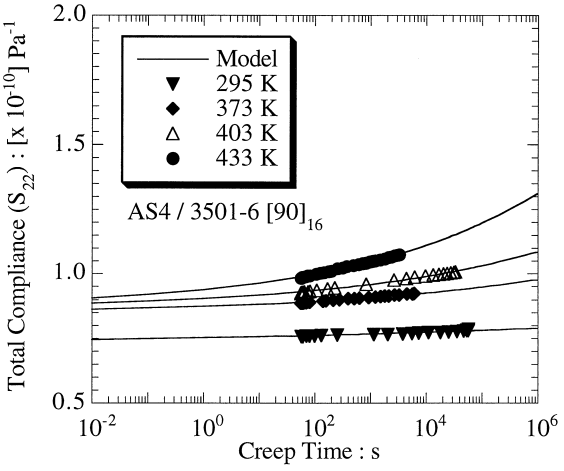

Fig. 10. Comparison of experimental and model fit transverse compliance of the composite at a creep stress of 31 MPa at 295 K and 29·7 MPa at 373, 403 and 433 K.

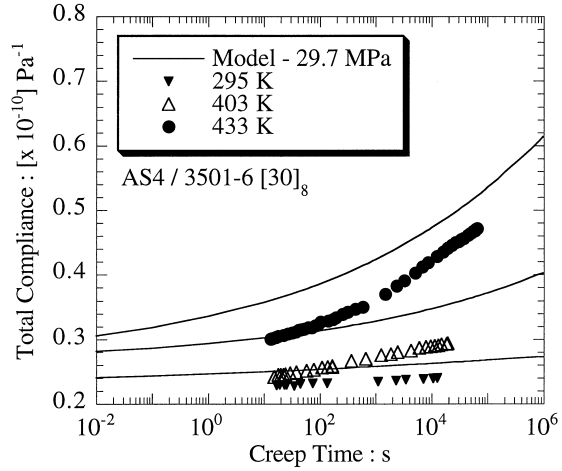

Fig. 13. Comparison of experimental and predicted compliance of the off-axis $[30]_8$ composite at a creep stress of 29·7 MPa.

numerically fitted, as per the procedure described in Section 2.2, by using eqn (13) and the above model parameters that were measured/derived experimentally. The activation volume was allowed to vary within the experimental scatter band to obtain the best fit as shown by the solid line in Fig. 15. The activation volumes used in the numerical fitting are shown in Figs 4–6 by broken lines. The numerical fit values for B and β for the epoxy, $[90]_{16}$ and $[10]_8$ composites are tabulated in Tables 8–10, respectively. Both B and β increase with increase in stress. B is a constant at a stress in the entire temperature range of investigation. The stress dependence of both B and β could not be obtained for epoxy and the $[90]_{16}$ composite since the results were limited to two stresses only. However, an exponential dependence[3] of B and β on stress and temperature was observed for the $[10]_8$ composite. Hence, an exponential function was used, during creep prediction for off-axis composites, to obtain the values of B and β at stress levels different from those in tabulated in Tables 8–10. The values of B and β for the composite were found to be smaller than those for the unreinforced epoxy.

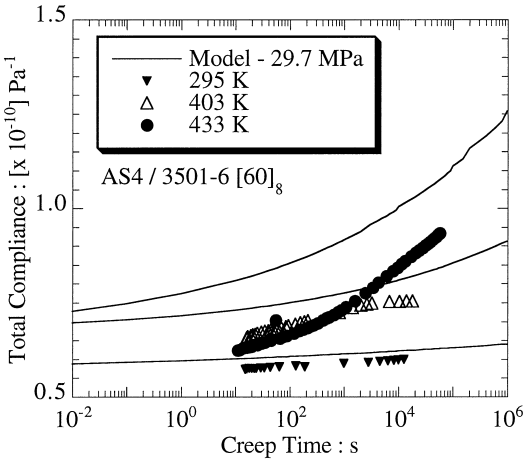

Fig. 14. Comparison of experimental and predicted compliance of the off-axis $[60]_8$ composite at a creep stress of 29·7 MPa.

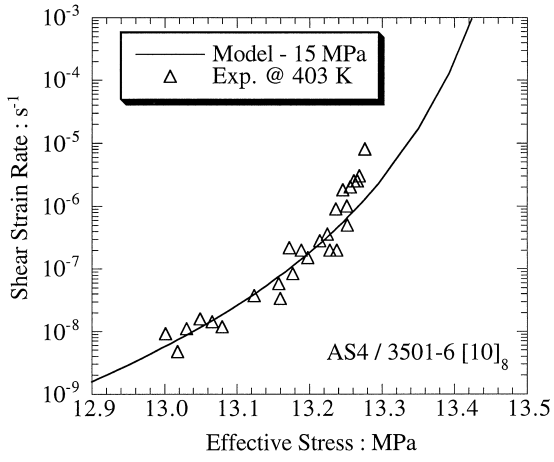

Fig. 15. Experimental and model fit shear creep rate as a function of effective stress for the composite at 403 K and at a creep stress of 15 MPa.

4.4.2 Comparison of results

In order to demonstrate the modeling capability of the creep model and the accuracy of numerical fitting used to obtain B and β, both the transverse and shear creep compliances of the composite were simulated by using eqn (13), the experimental activation energy, the activation volume and the numerical fit values for B and β. These calculated values are plotted in Figs 7–12 along with the experimental values. The excellent match between the simulated and experimental creep compliance values verifies the modeling capability and the accuracy of the numerical fitting used to obtain B and β.

Table 8. Creep model parameters obtained by numerical fitting of experimental creep results for 3501-6 epoxy, at two creep stresses (5 and 15 MPa), using eqn (13)

T (K)	B/βT (MPa^{-1} s^{-1})		β	
	at 5 MPa	at 15 MPa	at 5 MPa	at 15 MPa
295	—	$2{\cdot}99\times10^{31}$	—	0·073
373	$1{\cdot}04\times10^{8}$	$2{\cdot}89\times10^{31}$	0·061	0·138
403	$1{\cdot}29\times10^{8}$	$2{\cdot}98\times10^{31}$	0·066	0·155
433	$1{\cdot}09\times10^{8}$	$3{\cdot}07\times10^{31}$	0·059	0·217

Table 9. Creep model parameters obtained by numerical fitting of experimental creep results for AS4/3501-6 $[90]_{16}$ composite using eqn (13)

T (K)	B/βT (MPa^{-1} s^{-1})		β	
	at 15 MPa	at 29·7 MPa	at 15 MPa	at 29·7 MPa
295	$6{\cdot}43\times10^{20}$	$7{\cdot}14\times10^{27}$ [a]	0·048	0·067
373	$9{\cdot}6\times10^{21}$	$8{\cdot}75\times10^{27}$	0·082	0·113
403	$9{\cdot}0\times10^{20}$	$7{\cdot}52\times10^{27}$	0·072	0·126
433	$3{\cdot}96\times10^{20}$	$6{\cdot}21\times10^{27}$	0·084	0·135

[a]At a creep stress of 31 MPa.

Table 10. Creep model parameters obtained by numerical fitting of experimental shear creep results for AS4/3501-6 composite (using $[10]_8$ lay-up) using eqn (13)

T (K)	B/βT (MPa^{-1} s^{-1})		β	
	at 15 MPa	at 28·9 MPa	at 15 MPa	at 28·9 MPa
295	$4{\cdot}22\times10^{37}$	$2{\cdot}26\times10^{47}$ [a] $9{\cdot}3\times10^{58}$ [b]	0·050	0·053[a] 0·068[b]
373		$1{\cdot}28\times10^{41}$		0·086
403	$4{\cdot}19\times10^{37}$	$1{\cdot}27\times10^{41}$	0·124	0·096
433	$4{\cdot}57\times10^{37}$	$4{\cdot}35\times10^{39}$ [c]	0·122	0·111[c]

[a]At a creep stress of 42·0 MPa.
[b]At a creep stress of 66·3 MPa.
[c]At a creep stress of 20·8 MPa.

4.5 Creep prediction results

In the previous section, the creep prediction equation was verified to model the creep of AS4/3501-6 composites under in-plane shear loading and tensile loading. In order to verify the predictive capability of the creep prediction model in predicting the creep of the polymer composite and its epoxy matrix, the transverse, S_{22}, and shear compliance, S_{66}, results presented in the previous section were used to predict the time-dependent compliance of $[30]_8$ and $[60]_8$ composites. The experimental and predicted creep results for these composites are compared in this section.

4.5.1 AS4/3501-6 $[30]_8$ composite

At an applied creep stress of 29·7 MPa, the resolved in-plane shear stress is 12·9 MPa and the resolved transverse stress is 7·4 MPa. Total creep compliances S_{66} and S_{22} corresponding to these resolved stresses were determined[1] as a function of time by using the creep model and the model parameters given in the previous sections. β values used in the prediction correspond to values at 15 MPa as given in Tables 9 and 10. B values used in the prediction were obtained by extrapolating the values given in Tables 9 and 10 with an exponential function.[3] S_{11} at the resolved stress of 22·3 MPa was found to be independent of creep time[1] and its value is given by the inverse of the modulus values given in Table 3. From eqn (17), the Poisson's ratio of 0·31 and these values of S_{11}, S_{22} and S_{66}, the creep compliance of the $[30]_8$ composite was predicted in the temperature range from 295 to 433 K. These predicted values are compared with the experimental values in Fig. 13.

4.5.2 AS4/3501-6 $[60]_8$ composite

The experimental creep compliance curves obtained at various temperatures are given in Fig. 14. The smaller total compliance values, at the start of the creep, at 433 K than at 403 K is thought to be due to the discrepancy in the measured instantaneous strain. This will be discussed in Section 5. At an applied creep stress of 29·7 MPa, the resolved in-plane shear stress is 12·9 MPa and the resolved transverse stress is 22·3 MPa. Total creep compliances, S_{66} and S_{22}, corresponding to these resolved stresses were determined[1] as a function of time using the creep model and the model parameters given in previous sections. β values used in the prediction correspond to values at 15 MPa as given in Tables 9 and 10. B values used in the prediction were obtained by extrapolating the values given in Tables 9 and 10 using an exponential function.[3] S_{11} at the resolved stress of 7·4 MPa was taken to be independent of creep time since it was found to be independent of creep time at a much higher creep stress of 22·3 MPa. By using eqn (17), the Poisson's ratio of 0·31 and these values of S_{11}, S_{22} and S_{66}, the creep compliance of the $[60]_8$ composite was predicted in the temperature range from 295 to 433 K. These predicted values are compared with the experimental values in Fig. 14.

5 DISCUSSION

The objectives of this study were to develop a reliable creep model for polymer composites and to understand the influence of reinforcing carbon fibers on the viscoelastic properties of the epoxy matrix. Experimental and predicted creep results have been compared in the previous section. These creep results are discussed further in two separate sections to demonstrate how the objectives of this work have been realized.

5.1 Modeling and predictive capability of the creep model

The experimental creep data for the unidirectional composite and its epoxy matrix were numerically fitted to the creep model presented in this paper by using eqn (13), the experimentally determined activation energy and the activation volume, as per the procedure discussed in Section 2.2. The experimental creep data and the model fit lines are compared in Figs 7–12 for both epoxy and composites. Both data sets agreed within 3% error in a wide range of stress (10–80% of the ultimate tensile strength) and temperature (295–433 K), thus demonstrating the modeling capability of the creep model and its applicability to model both the composite and its polymer matrix. The numerical fit values of model parameters B and β are consistent with respect to their dependence on stress and temperature. They are discussed further in the next section. The broken lines in Figs 4–6 indicate that the activation volume values used in the modeling of creep data are almost same at all temperatures. This supports the apparent temperature independence of experimental activation volume data and the procedure followed in this paper to allow the activation volume to vary within the scatter band. Further experimentation is needed to understand whether such a scatter is inherent or a result of the experimental procedure adopted in this study to determine the activation volume.

The predictive capability of this creep model was tested by comparing the predicted and experimental compliance results for off-axis $[30]_8$ and $[60]_8$ composites, as shown in Figs 13 and 14. From these figures it can be inferred that the predicted compliances were in good qualitative (i.e. similar shape) agreement with the experimental results. However, the predicted values at a given creep time were higher than the experimental results by 15 to 23%, depending on the temperature and fiber orientation. The predicted values seem to have been shifted up along the ordinate axis representing the creep compliance. One possible explanation for this is the difference in the predicted and experimentally measured instantaneous strain values. Since the S_{11}, S_{22} and S_{66} compliances used in the prediction of the creep compliance of off-axis composites were based on creep data from a single creep test at a representative stress and temperature, establishing the statistical range in the creep data by using multiple specimens or tests at each

stress and temperature may help verify the accuracy of predictions of the creep model developed in this paper. Similarly, the experimental creep data for off-axis specimens need to be generated with multiple specimens. Moreover, the accuracy of prediction can be improved further by determining accurately the stress and temperature dependence of B and β by performing creep tests and subsequent modeling, at more stress levels at a given temperature.

5.2 Influence of reinforcing carbon fibers on the creep of epoxy matrix

A detailed discussion on this can be found in.[1,20] Activation energies tabulated in Table 1 for the unreinforced epoxy and the $[90]_{16}$ and $[0]_8$ composites agree within $5\,kJ\,mol^{-1}$. This suggests that the creep mechanism is the same in both the epoxy and its composite and that it is unaltered by the reinforcing fibers. These activation energies correspond to α transition in the matrix in the investigated temperature range. The success in usage of this activation energy to model the temperature dependence of the creep of the composite suggests that the creep of the composite is due to the mechanism that causes α transition in the epoxy matrix. Higher activation energy values obtained for $[10]_8$ and $[45]_8$ composites, wherein both tensile and shear strains are induced by the applied stress, indicate that the activation energy for creep under shear loading may be different from the activation energy for creep under tensile loading.

From Table 7, it can be inferred that the activation volume values for the epoxy falls within the bounds for the $[90]_{16}$ composite. Hence, it can be surmised that both the epoxy and the $[90]_{16}$ composite have the same activation volume at an effective stress. This supports the above conclusion that the reinforcing carbon fibers do not alter the creep mechanism of the epoxy matrix, and this is consistent with the same activation energy obtained for both the materials.

The instantaneous modulus of the epoxy is increased by a factor of 2·6 by the reinforcing carbon fibers. At 0·62 volume fraction of fibers, the matrix is confined to interfiber spacing which is of the order of μm. Owing to the Poisson's ratio mismatch (0·2 for the fiber and 0·37 for the epoxy at 295 K), the matrix will be constrained during transverse tensile loading from contracting in a direction parallel to the fiber axis. This would result in a stiffening of the $[90]_{16}$ composite as compared with pure epoxy matrix. By using the modulus of the AS4 fiber (248 GPa) and the resin (5·22 GPa at 295 K) and 0·62 for the volume fraction of fibers, the modulus of the $[90]_{16}$ composite at 295 K is computed to be 13·3 GPa, by simple inverse rule of mixtures, which is less than the experimental value of 13·49 GPa (measured at $10^{-4}\,s^{-1}$) by 1·6%. However, since the simple inverse rule of mixtures[18] does not take into account the Poisson's ratio mismatch, a more rigorous, generalized, self-consistent field model of Christensen and Lo[21] was also used and this resulted in a transverse modulus of 15·71 GPa, which is 16·5% higher than the experimental value of 13·49 GPa. The properties for AS4 fiber used for this computation were taken from.[22] The above results suggest that the increase in instantaneous modulus value for the epoxy may be due to the volume replacement effect of the fibers without any additional stiffening caused by the constraint (owing to Poisson's ratio mismatch) placed on the epoxy matrix by the surrounding fibers.

However, this constraint effect becomes much more influential at temperatures above the T_g, when the matrix becomes incompressible ($\nu_m = 0{\cdot}5$). By comparing the rubbery moduli of the epoxy and the $[90]_{16}$ composite in Tables 2 and 5, it can be observed that the rubbery modulus of the epoxy is increased by a factor of 31 upon reinforcement. From the modulus of the AS4 fiber (248 GPa) and the resin (0·063 GPa at 552 K) and 0·62 for the volume fraction of fibers, the modulus of the $[90]_{16}$ composite at 558 K is computed to be 0·17 GPa by simple inverse rule of mixtures· The measured value of 1·82 GPa is higher than this value obtained by simple rule of mixtures by a factor of 11. The generalized self-consistent field model yields a value of 0·76 GPa, still less than the experimental value by a factor of 2·4. Hence, it can be concluded that the interaction between the epoxy and the carbon fibers (such as fiber/matrix adhesion) may play an role in reinforcing the epoxy in addition to the reinforcement by simple volume replacement effect and constraint due to Poisson's ratio mismatch. Galanti and Sperling[23] observed an increase in Young's modulus of silicone rubber by a factor of 8 when reinforced with 0·15 volume fraction of silica fillers. They correlated this increase in modulus to an increase in internal energy of the silicone rubber due to the reinforcing fillers. They reasoned that this increase in internal energy could be due to such causes as crystallization of polymer at the filler surface, stretching of hydrogen bonds, decoupling of aggregated filler particles, plastic deformation of filler particles, formation of crazes or microvoids, or a combination of several of these. Similar such fiber/matrix interactions (e.g. fiber/matrix adhesion) are believed to have influenced the retardation/relaxation behavior of the epoxy, leading to an increase in T_g by 5 to 6 K depending on the orientation of the continuous carbon fibers to the loading axis except in the $[10]_8$ composite where an increase by 11 K was observed. Similarly, a decrease in the T_β by 6 to 8 K was also observed during sub-zero β transition due to matrix/fiber interactions. Such an increase in the T_g and a decrease in the T_β of polymers as a consequence of reinforcing particulate fillers has been observed by many investigators in the past. A comprehensive review of these studies can be found in.[24]

A consequence of this stiffening of the instantaneous and rubbery moduli of epoxy due to reinforcement is a reduction in the magnitude of creep. This is borne out by the creep results. Comparing the creep compliance

results for the epoxy and $[90]_{16}$ composite given in Figs 8 and 9, it can be observed that, during a creep time of 10^6 s, the increase in epoxy compliance is 33% while that for the $[90]_{16}$ composite is only 9·4%. The magnitude of creep is also less than the that of the $[90]_{16}$ composite. For example, the total creep strain over a period of 10^4 s at 403 K is 0·1% for the epoxy and 0·02% for the $[90]_{16}$ composite. The above results confirm that the reinforcing carbon fibers significantly alter the creep behavior (which corresponds to the creep magnitude and creep rate) of the epoxy matrix.

Finally, comparing the values of B and β for the epoxy and $[90]_{16}$ composite in Tables 8 and 9, it can be observed that B and β for the epoxy decrease due to reinforcement. In eqn (13) all the terms except X_0 are constant. Hence, a decrease in B is thought to be due to an increase in X_0 and vice versa. Here, the reader is reminded that X_0 and β define the Weibull distribution in X, which is the total change in N_1 from the start of creep until a certain creep stage is reached. An increase in B and an increase in β would mean a narrowing of the Weibull distribution. Conversely, a decrease in B and a decrease in β would mean a broadening of the distribution. Hence, an increase in X_0 (i.e. a decrease in B) and a decrease in β observed for epoxy as a result of reinforcement is interpreted as being due to a broadening of the distribution in X. In other words, the reinforcing carbon fibers reduce the cooperative chain segmental mobility in the epoxy, causing a broadening in the distribution in X and subsequently a reduction in creep rate. Such broadening of the distribution in X is also believed to be the reason for the increase in T_g upon reinforcement.

6 CONCLUSIONS

A creep model has been developed to model and predict creep of a thermo-rheologically complex, high-T_g epoxy and its carbon-fiber-reinforced composite. Good modeling capability of the creep model has been demonstrated for unidirectional composites in the temperature range 295–433 K and at stress levels of up to 80% of the composites' ultimate tensile strength. The predictive capability of the model has been verified by good qualitative (i.e. shape) agreement and reasonable quantitative agreement of the predicted results (higher by 15–23%) with the experimental creep data for off-axis composites in the same temperature range mentioned above. The creep of the epoxy and its composite, in the temperature range 295–433 K, has been found to be due to the mechanism causing α transition in the epoxy matrix, and the average activation energy for this mechanism is 494 kJ mol^{-1}. The reinforcing fibers do not alter the creep mechanism in the epoxy (as suggested by the similar activation energies for both the epoxy and composites) but do alter the creep behavior (i.e. reduce the creep magnitude and creep rate) by increasing the resistance to cooperative chain segmental mobility of the polymer chain segments (as suggested by the widening of the Weibull distribution in X) and by stiffening the matrix.

ACKNOWLEDGEMENTS

This work was sponsored by the Office of Naval Research under contract N00014-89-J-3048. The authors would like to thank Dr Peter Thornley, Dr Jeff Meyer and Dr Daan Feng of Amoco Chemical Company, Naperville, Illinois, for their help in DMTA testing. Also, the authors would like to acknowledge the help of Professor I. M. Daniel for allowing us to use his laboratory facilities, and the excellent technical assistance of Mr M. Seniw, Mr A. Bilyk and R. Kramer at Northwestern University.

REFERENCES

1. Raghavan, J., Creep and creep rupture of carbon fiber reinforced polymer composite. Ph.D. thesis, Northwestern University, Evanston, Illinois, 1994.
2. Raghavan, J. and Meshii, M., Prediction of creep rupture of unidirectional carbon fiber reinforced polymer composite. *Mater. Sci. Eng. A,* 1995, **197**, 237–249.
3. Raghavan, J. and Meshii, M., Creep rupture of polymer composites. *Compos. Sci. Technol.,* 1997, **57**, 375–388.
4. Ward, I. M. and Hadley, D. W., *An Introduction to the Mechanical Properties of Solid Polymers*. John Wiley and Sons, New York, 1993, p. 93.
5. Conrad, H., Thermally activated deformation of metals. *J. Met.,* 1964, **16**(7), 582–589.
6. Krausz, A. S. and Eyring, H., *Deformation Kinetics*. John Wiley and Sons, New York, 1975.
7. Raghavan, J. and Meshii, M., Activation theory for creep of matrix resin and carbon fiber reinforced polymer composite. *J. Mater. Sci.,* 1994, **29**, 5078–5084.
8. Matsuoka, S., *Relaxation Phenomena in Polymers*. Oxford University Press, New York, 1992.
9. Eyring, H. and Halsey, C., The mechanical properties of textiles III. *Text. Res. J.,* 1946, **16**, 13–25.
10. Basinski, Z. S., Activation energy for creep of aluminum at sub atmospheric temperatures. *Acta Metall.,* 1957, **5**, 684–686.
11. Conrad, H. and Weidersich, H., Activation energy for deformation of metals at low temperatures. *Acta Metall.,* 1960, **8**, 128–130.
12. Fotheringham, D. G. and Cherry, B. W., The role of recovery forces in the deformation of linear polyethylene. *J. Mater. Sci.,* 1978, **13**, 951–964.
13. Kubat, J., Rigdhal, M. and Selden, R., Internal stresses and activation volumes from the stress relaxation behavior of polyethylene at low deformations. *J. Appl. Polym. Sci.,* 1976, **20**, 2799–2809.
14. Pink, E. and Campbell, J. D., Deformation characteristics of reinforced epoxy resin, Part I. Mechanical properties. *J. Mater. Sci.,* 1974, **9**, 658–664.
15. Pink, E. and Campbell, J. D., Deformation characteristics of reinforced resin, Part II. An analysis of thermally activated deformation. *J. Mater. Sci.,* 1974, **9**, 665–672.
16. White, J. R., Stress relaxation in polymers: a modified site analysis. *Mater. Sci. Eng. A,* 1980, **45**, 35–42.

17. Dougherty, R. E., *Probability and Statistics for the Engineering Computing and Physical Sciences*. Prentice Hall, New Jersey, 1990.
18. Hull, D., *Introduction to Composite Materials*. Cambridge University Press, Cambridge, 1981.
19. Raghavan, J. and Meshii, M., Prediction of creep and creep rupture of unidirectonal carbon fiber reinforced polymer composite and its expoxy matrix. Part I: Creep. In *Proc. Int. Symp. on High Performance Composites—Commonality of Phenomena*, ed. K. K. Chawla, P. K. Liaw and S. G. Fishman. TMS/ASM, Illinois, 1994, pp. 495–515.
20. Raghavan, J., Meshii, M. and Feng, D., Influence of reinforcing carbon fibers on the viscoelastic properties of the epoxy matrix. *Polym. Compos.,* 1997, **18**, 55–63.
21. Christensen, R. M., A critical evaluation for a class of micro-mechanics models. *J. Mech. Phys. Solids,* 1990, **38**, 379–404.
22. Adams, D. F., Zimmermann, R. S. and Odom, E. M., Polymer matrix and graphite fiber interface study. Report UWME-DR-501-102-1, University of Wyoming, 1985.
23. Galanti, A. V. and Sperling, L. H., Relationship between thermoelasticity and reinforcement in elastomers: silica filled silicone elastomers. *Polym. Eng. Sci.,* 1970, **10**, 177–184.
24. Manson, J. and Sperling, L. H., *Polymer Blends and Composites*. Plenum Press, New York, 1976.